Soft Science

Research Article

Shape memory behaviors of 3D printed liquid crystal elastomers

Lu Dai[1], Liqian Wang[2], Baihong Chen[2], Zengting Xu[2], Zhijian Wang[3,*], Rui Xiao[2,*]

[1]School of Civil Engineering and Architecture, Zhejiang Sci-Tech University, Hangzhou 310018, Zhejiang, China.
[2]State Key Laboratory of Fluid Power & Mechatronic System, Key Laboratory of Soft Machines and Smart Devices of Zhejiang Province, Zhejiang University, Hangzhou 310027, Zhejiang, China.
[3]Key Laboratory of Aerospace Advanced Materials and Performance Ministry of Education, School of Materials Science and Engineering, Beihang University, Beijing 100191, China.

[*]**Correspondence to:** Prof. Zhijian Wang, Key Laboratory of Aerospace Advanced Materials and Performance Ministry of Education, School of Materials Science and Engineering, Beihang University, Beijing 100191, China. E-mail:zhijianw@buaa.edu.cn; Rui Xiao, State Key Laboratory of Fluid Power & Mechatronic System, Key Laboratory of Soft Machines and Smart Devices of Zhejiang Province, Zhejiang University, Hangzhou 310027, Zhejiang, China. E-mail: rxiao@zju.edu.cn

Abstract

As soft active materials, shape-memory polymers (SMPs) and liquid crystal elastomers (LCEs) have attracted considerable research interest due to their potential applications in various areas. SMPs refer to polymeric materials that can return to their permanent shape in response to external stimuli, such as heat, light, and solvent. In this sense, LCEs can exhibit intrinsic shape-memory behaviors since LCEs can switch between two shapes with temperature change due to the order-disorder transition of liquid crystals. In this work, we fabricate both the polydomain and monodomain nematic LCEs through direct ink writing 3D printing. With increasing the temperature of the substrates, the printed LCEs change from the monodomain state to the polydomain state. For polydomain LCEs, a reversible shape change can occur upon constant loading, while the monodomain can switch the shape with temperature in the stress-free state. This two-way shape-memory behavior is caused by the nematic-isotropic phase transition. We further show that the printed LCEs exhibit a good one-way shape-memory effect due to glass transition. The shape recovery region increases with the programming temperature, which is a typical temperature memory effect. Finally, it is demonstrated that complex shape-memory performance can be designed by combining one-way and two-way shape-memory effects. Specifically, for the monodomain LCEs, with increasing temperature, the programmed shape first recovers, and a second shape change can further occur due to the nematic-isotropic transition.

INTRODUCTION

Shape-memory materials, such as shape-memory polymers (SMPs), and shape-memory alloys (SMAs), can recover from a temporary programmed shape to the original shape upon external stimulus[1,2]. Compared with SMAs, SMPs have several advantages. They can sustain large deformation and show responsiveness to multiple stimuli[2,3]. Due to the broad potential applications in biomedical and aerospace areas, SMPs have received considerable attention in the past two decades[4-10]. The shape-memory effect has been reported and optimized in various polymeric systems to improve the performances of shape fixity and shape recovery[11,12]. Regarding the fabrication process, earlier works focus on traditional methods, such as molding, extrusion, and electrospinning[13]. The development of the 3D printing technique provides the possibility to design devices with complicated geometries[14-20]. For example, Lin *et al*. adopted direct ink writing (DIW) 3D printing to fabricate remotely controllable shape memory occlusion devices by incorporating magnetic particles into the polymer matrix[16]. Zhang *et al*. employed the digital light processing (DLP) technique to fabricate deployable solar panels[14].

The typical thermally-activated shape memory process starts with programming a temporary shape and cooling it down to a low temperature to fix it. Upon heating, the temporary shape can be recovered to the permanent shape in a stress-free state. This is named a one-way shape-memory effect, which means that the temporary shape has to be reprogrammed once shape recovery is complete. In contrast, a two-way shape-memory effect represents that the polymers can switch repeatably between two shapes with changing temperatures while no reprogramming is needed. The two-way shape-memory effect is mainly realized in semicrystalline polymers based on the melting transition[21,22]. The early works showed that the two-way shape-memory effect needs to be achieved under constant applied stress[23]. Behl *et al*. and Song *et al*. have further demonstrated that the two-way shape-memory effect can also be obtained without external loading, which requires a broad melting transition region and a training process[24,25]. Namely, the samples with a programmed strain at a programming temperature T_{prog} need to be cooled to a low temperature T_{low}. The shape switch is achieved between a median temperature T_{mid} and T_{low}. The reversible strain in these material systems is relatively low, with a typical magnitude of 20%.

Liquid crystal elastomers (LCEs) are composed of liquid crystal mesogens and polymer networks. Thus, they can exhibit both the behaviors of elastic rubbery networks and anisotropic properties of liquid crystals[26,27]. The reversible shape change is achievable due to the order-disorder transition of liquid crystals. For monodomain nematic LCEs, a large anisotropic shape transition can occur with temperature change. In contrast, shape change can only occur upon an external load for polydomain LCEs[28]. Nevertheless, LCEs are ideal candidates as two-way SMPs, which can be further used as artificial muscles, sensors, and actuators[29]. Fuchi *et al*. showed that specific reversible folding structures can be designed by controlling the distribution and orientations of directors in LCEs[30]. Roach *et al*. demonstrated that the liquid crystal fibers can mimic the bicep muscles with large activation strain and stress[31].

It is challenging for traditional manufacturing methods to fabricate large LCE samples with the desired alignments of liquid crystal mesogens[32]. The alignment can be realized through mechanical stretching[28], electric field[33], *etc*. A new polymer network is needed to be formed to fix these alignments. Yackcki *et al*. used a two-step polymerization approach to synthesize LCEs[28]. The first step is used to obtain polydomain LCEs, which are further aligned using mechanical loading. Due to the excess of reaction groups, a second

polymerization can occur to fix the aligned mesogens. The dynamic covalent network approach is also widely adopted to form the new relaxed polymer network[34,35]. The development of 3D printing has provided a solution to fabricating the LCEs with complex geometries. For the DIW technique, the shear force in the extrusion process results in the alignment of the mesogens along the printing direction, while the photo-cross-linking process fixes the orientation of the mesogens[36]. The DIW technique is currently the most widely adopted printing method for LCEs. The DLP technique has also been employed to fabricate LCEs but mostly for polydomain LCEs. For example, Traugutt *et al.* employed the DLP technique to print LCE-based metamaterials in the polydomain states, which show a significantly improved energy absorption ability[37].

It should be recognized that the two-way shape-memory effect originates from the order-disorder phase transition. With changing temperatures, it is observed that the glass transition or melting transition can also appear in the LCEs[38-40]. Thus, these LCEs should also exhibit the one-way shape-memory effect. However, this has not been extensively investigated. In this work, we fabricate both polydomain and monodomain LCEs through DIW 3D printing. We further demonstrate that these LCEs exhibit both one-way and two-way shape-memory behaviors. It is also shown that complex shape recovery paths can be achieved by combining the two effects.

EXPERIMENTAL METHODS
Materials
The printing ink was prepared through the Michael addition reaction between liquid crystal mesogen RM257(1,4-Bis-[4-(3-acryloyloxypropyloxy) benzoyloxy]-2-methylbenzene, Hwrkchemical, 98%) and chain extender EDDET(2,2′- (ethylenedioxy) diethanethiol, Sigma-Aldrich, 95%). The RM257 (8.2404 g, 14 mmol) was first dissolved in 50 mL of CH_2Cl_2 solvent. The EDDET (2.1876 g, 12 mmol) and dipropylamine (as catalyst, 0.100 g, 1 mmol, Sigma-Aldrich, 99%) were further added into the above mixture solution. The solution was stirred at room temperature overnight. The photo-initiator (2-hydroxyethoxy)-2-methypropiophenone (Irgacure 2959) (0.500 g, 0.2 mmol, Sigma-Aldrich, 98%) was added into the solution. The mixture solution was heated in an oven at 85 °C for 24 h to allow complete evaporation of the solvent and loaded into a syringe. In the above process, the RM257 is added with an excessive amount to produce the oligomer with the acrylate groups as the end groups. The linear oligomers would be extrudable. After being extruded and loaded onto the substrate, the LCE filament is further cured under UV light in the presence of the photoinitiator, leading to the formation of the polymer network. This recipe has been widely studied and adopted in the DIW printing techniques of LCEs[26,32].

The customized 3D printing system is composed of an extrusion system and a 3D positioning stage, as shown in Figure 1. The extrusion system consists of an air pump, a pressure controller, and a multi-nozzle printing head. In the printing process, the LCE ink was extruded out of nozzles onto a glass substrate at 40 °C to obtain monodomain LCEs or 80 °C for polydomain LCEs. Continuous illumination of 365 nm UV light-emitting diodes (LEDs) was applied during printing. The nozzle moving speed, the extrusion pressure, and the inner diameter of the nozzle were fixed at 3 mm/s, 800 kPa, and 0.8 mm, respectively. After printing, the structures were further cured under a 365 nm UV light (UVP crosslinker, CL-3000L, 2066 W) for 30 mins.

Characterization
Differential scanning calorimetry
The differential scanning calorimetry (DSC) test was carried out using a TA DSC 25. The specimens of 3D printed polydomain and monodomain LCEs with a weight of 5 mg were first equilibrated at -30 °C for 5 mins. The temperature was then ramped to 100 °C at 5 °C /min.
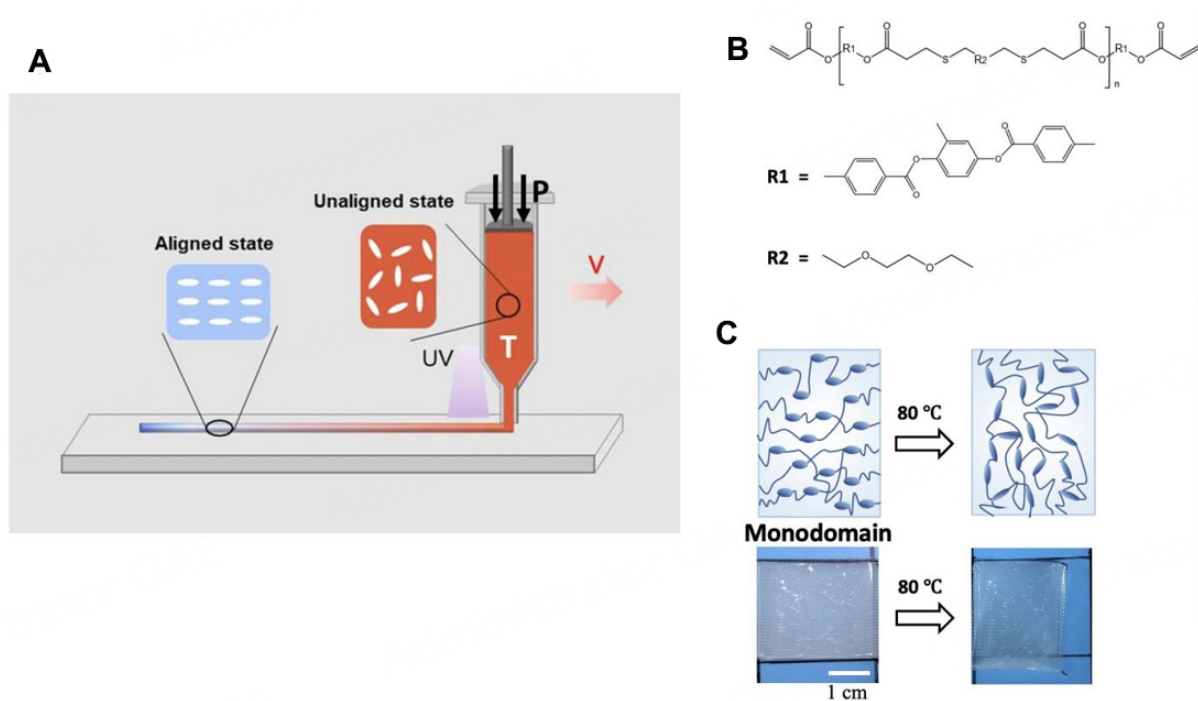
Figure 1. (A)Schematic diagram of the 3D printing process, (B) the molecular structure of uncrosslinked liquid crystal oligomer, and (C) the printed LCE specimens with thermally-responsive behaviors. The appearance of as-printed polydomain LCEs shows no difference from the monodomain LCEs. However, the shape remains unchanged for the polydomain LCEs with changing temperatures. LCEs: Liquid crystal elastomers.

Dynamic temperature sweep
The following tests were all performed on the dynamic mechanical analyzer TA Q800 for both polydomain and monodomain LCEs. The rectangular specimens with a size of 12 mm× 5 mm × 1 mm were used. The same size of specimens was also used for the thermal actuation and shape-memory tests. The specimen was first equilibrated at -40 °C for 5 mins. A dynamic strain of 0.2% at a frequency of 1 Hz was further applied. The temperature was then increased to 100 °C at 3 °C /min.

Thermal actuation behaviors
To characterize the thermal actuation behaviors of LCEs, the specimens were first equilibrated at 150 °C for 5 mins. A force was then applied at a constant rate for 1 min to reach the target force level. The temperature was then decreased to -30 °C at 3 °C/min. For polydomain LCEs, the applied stress was chosen as 0 kPa, 20 kPa, and 50 kPa, while for monodomain LCE, the specimen was subject to 0 kPa or 50 kPa during the cooling process.

Shape-memory behaviors
The shape-memory cycle was performed as follows. For polydomain LCEs, the specimens were first equilibrated at either 10 °C or 50 °C. A force was applied at a constant rate for 1 min. For the case of deformed at 10 °C, the final stress was set as 100 kPa, while for the 50 °C, the value was set as 20 kPa. The temperature was then decreased to -30 °C at 10 °C /min. The force was then decreased to zero within 1 min. The temperature was further increased to 100 °C at 3 °C /min.

For monodomain LCEs, the specimens were loaded to the DMA in the perpendicular direction of the alignment of the mesogens. The specimens were first equilibrated at 10 °C for 5 mins. A force was applied at a constant rate for 1 min to reach a final stress of 150 kPa, 200 kPa, and 250 kPa. Similarly, the temperature was decreased to -30 °C at 10 °C /min, and the force was then unloaded. The shape change was monitored during the heating process with the temperature increased to 150 °C at 3 °C /min.

We also fabricate a bilayer structure with a length of 4 mm and a width of 1 mm. The polydomain layer has a thickness of 0.6 mm, and the monodomain layer has a thickness of 0.3 mm. The monodomain layer is printed along the 45° direction with respect to the length direction. The as-printed flat specimen was bent to an arc shape and then placed in the fridge set at -15 °C to fix the temporary shape. The specimens were then taken out and placed on a hot plate. The shape was observed by changing the temperature of the hot plate.

RESULTS AND DISCUSSION

The extrusion process of 3D printing can effectively align the mesogens. The rotation of mesogens in random directions has been significantly affected by the temperature of the glass substrate. After being extruded, the uncrosslinked LCE filaments are loaded on a substrate. When the temperature of the substrate is high, the liquid crystal mesogens rotate quickly, leading to a randomly oriented state before crosslinking. After UV illumination, the LCE filaments are obtained in a polydomain state. In contrast, when the temperature of the substrate is low, the liquid crystal mesogens rotate slowly, and the alignment could be fixed by the newly formed crosslinking network under UV light, resulting in a monodomain state. In the experiments, we print the polydomain and monodomain LCEs with the temperature of substrate as 80 °C and 40 °C, respectively. The DIW 3D printing technique to fabricate LCEs has also been adopted by several groups[26,41] to achieve complex shape-morphing structures.

The DSC technique is used to characterize the phase transition behaviors of 3D printed LCEs, which has been demonstrated as an efficient method to reveal the melting transition, glass transition, and nematic-isotropic transition in polymers[42]. As shown in Figure 2, heat capacity increases quickly from -20 °C to 5 °C, corresponding to the glass transition. A similar glass transition region is also observed in monodomain LCEs. An additional small change of the heat capacity appears in the temperature region between 50 °C to 70 °C for monodomain LCEs due to the nematic-isotropic transition, which cannot be observed in polydomain LCEs. As shown, the change in heat capacity due to the nematic-isotropic transition is less noticeable compared with the change during the glass transition.

Dynamic mechanical analysis (DMA) is widely used to characterize SMPs. For both semicrystalline and amorphous SMPs, the modulus changes dramatically with temperature, which is, in fact, the underlying physical mechanism of the shape-memory effect. As shown in Figure 3, the temperature-dependent dynamic properties (storage modulus and loss factor tan*δ*) are similar to those of chemically cross-linked polymer networks. The modulus decreases by a magnitude of three from 2 GPa to 1 MPa with increasing temperature. The equilibrium rubbery modulus of monodomain LCEs is higher than that of the polydomain LCEs. This can be caused by the dimension change of monodomains in the heating process. The alignment of polymer chains may also affect the modulus, as discussed in Linares *et al.*[43]. The glass transition temperature defined as the peak of tan*δ* is 11 °C for polydomain LCEs and 14 °C for monodomain LCEs. It is noticed that the glass transition region measured by the DMA shifts to a higher temperature compared with that obtained from DSC, which is also observed in various polymer systems[44]. The value of tan*δ* decreases in a more gradual manner compared with traditional amorphous SMPs, probably due to the influence of mesogens. Different from the DSC results, it is hard to distinguish the nematic-isotropic transition from the DMA results.
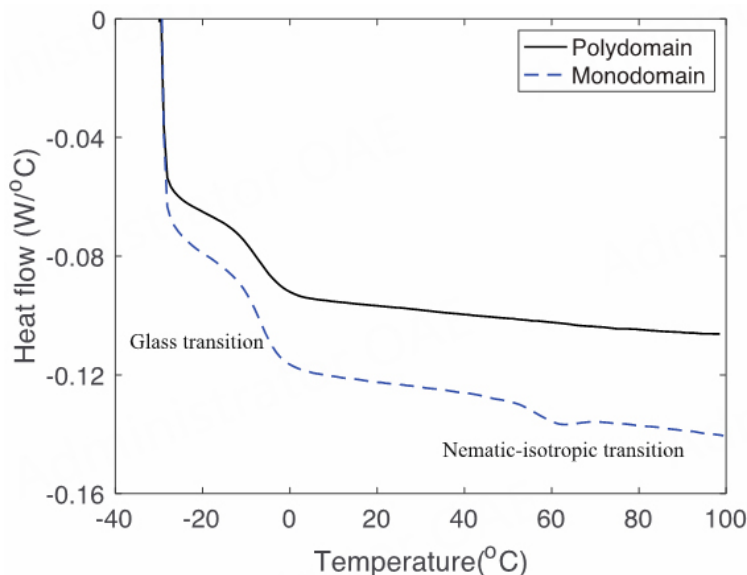
Figure 2. Heat flow as a function of temperature for 3D printed polydomain and monodomain LCEs measured through differential scanning calorimetry. LCEs: Liquid crystal elastomers.
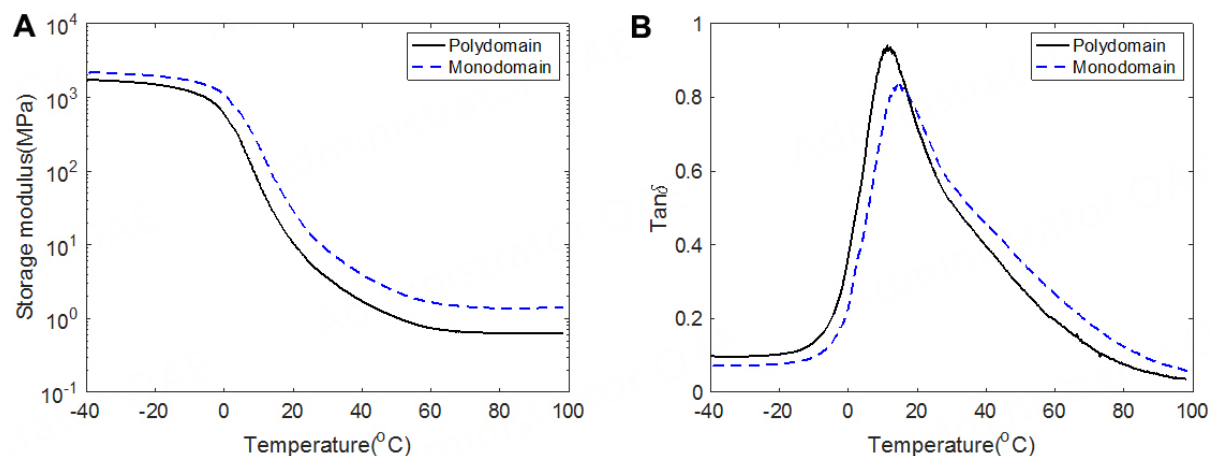
Figure 3. The dynamic properties of (A) storage modulus and (B) loss factor tanδ of polydomain and monodomain LCEs obtained from dynamic temperature sweep tests. LCEs: Liquid crystal elastomers.

Figure 4 plots the thermal actuation behaviors of polydomain and monodomain LCEs with different magnitudes of applied stress. Strain is defined as $\epsilon = (L - L_0)/L_0$, where L is the length of specimens at the current time and L_0 is the equilibrium length of the specimens at the high temperatures without force applied. For polydomain LCEs, strain remains at a low level during the cooling process when no force is applied. However, when a small amount of stress is applied, for example, 20 kPa, a clear shape change occurs with cooling. The resultant strain can reach as high as 0.6. This shape change is caused by orientation of the mesogens along the loading direction induced by the applied stress. In contrast, a clear shape change can be observed for monodomain LCEs when no force is applied. This shape change in the stress-free state is caused by the nematic-isotropic transition. At low temperatures, the mesogens are aligned in the same direction, which is named the nematic state. With increasing temperature, the entropic effect dominates. The directions of mesogens switch from the aligned state to the random state, resulting in an isotropic state. This further leads to a change in shape. For both polydomain and monodomain LCEs, the final strain
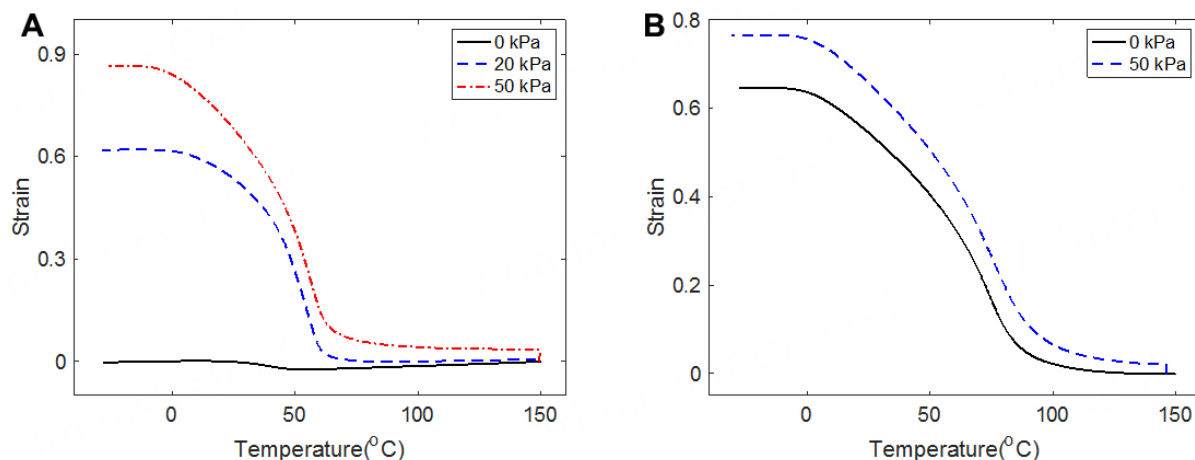
Figure 4. Thermally-activated shape change of (A) polydomain and (B) monodomain LCEs under different applied stress levels. LCEs: Liquid crystal elastomers.

increases with the applied stress. Yakacki *et al.* have used a two-stage Michael addition and photo-polymerization reaction to synthesize acrylate-based LCEs. Similar phenomena have also been observed[28].

The above experimental results have shown that the monodomain LCEs can switch between two shapes when the temperature changes. This behavior is the same as the two-way shape-memory behaviors observed in semicrystalline polymers[22], though the inherent physical mechanism is different. For semicrystalline polymers, the two-way shape-memory effect is caused by the melting transition, while it is caused by the nematic-isotropic transition for monodomain LCEs. As shown in Figures 2 and 3, the 3D-printed LCEs also have a clear glass transition behavior. Thus, they should also exhibit the classic one-way shape-memory effect. Motivated by this, the polydomain LCEs have been subjected to a typical shape-memory cycle, as shown in Figure 5. The temporary shape is formed by applying a force at a certain temperature, cooled down to a low temperature, and unloaded to a stress-free state. The permanent shape can be further fully recovered with increasing temperature.

We have employed two different programming conditions. When programmed at a higher temperature, a lower stress can actually result in a larger programmed strain. Here, the stress is chosen to achieve a strain of about 20%-30%. However, to quantitatively compare the effects of programming temperature, the strain is further normalized by the maximum programmed strain. As shown in Figure 6, shape recovery occurs in a lower temperature region when the programming temperature is also lower. This effect is named the temperature memory effect for traditional SMPs[45]. Here, we demonstrate that the same effect can also occur in the LCEs. For amorphous polymers, the temperature memory effect is caused by the fact that the temporary shape is fixed by different relaxation mechanisms. Here, from the recovery region, it is possible that the fixity of the temporary shape is not significantly evolved with the rotation of mesogens when the deformation temperature is low. In contrast, when programmed at higher temperatures, the shape recovery region is consistent with the region of the nematic-isotropic transition region, as shown in Figure 4A. Thus, it is reasonable to conclude that the temporary shape formed in this condition is mainly caused by the rearrangement of mesogens due to the phase transition. Our preliminary study also shows that a further increase of the programming temperature above 50 °C only has a limited effect on the shape recovery region.
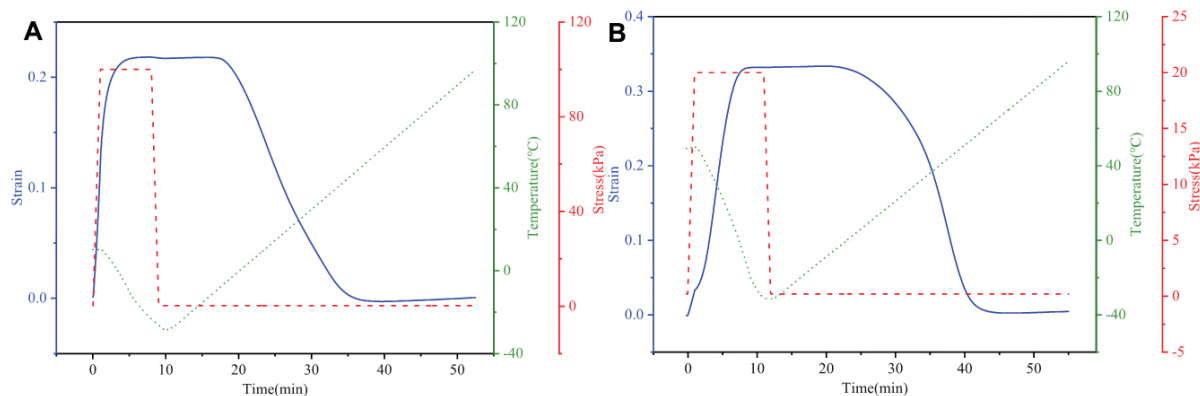
Figure 5. Shape-memory cycles for polydomain LCEs programmed under different conditions: (A) 10 °C and 100 kPa and (B) 50 °C and 20 kPa. LCEs: Liquid crystal elastomers.
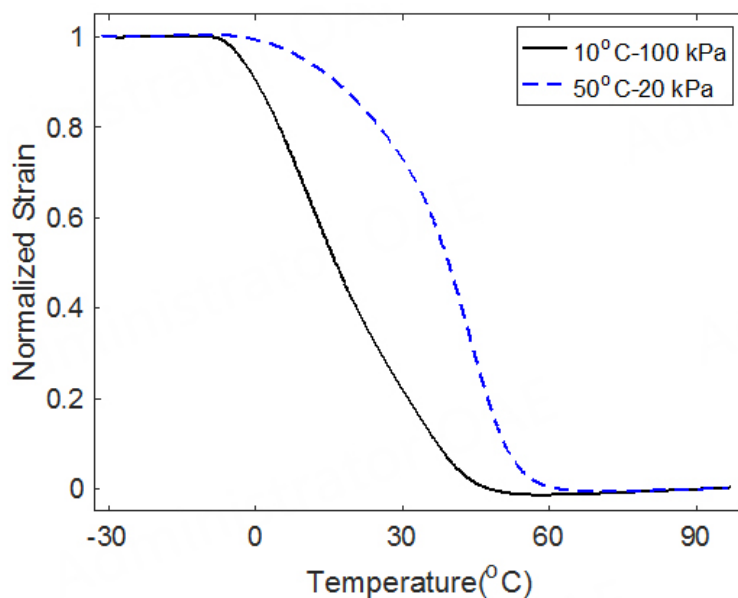
Figure 6. Comparison of the shape recovery performance of polydomain LCEs programmed at different temperatures. LCEs: Liquid crystal elastomers.

For the monodomain LCEs, we investigate the one-way shape-memory effect in the perpendicular direction of the printed direction. If the deformation is applied along the printed direction, it will not be able to distinguish the shape change caused by shape recovery and thermal actuation induced by the nematic-isotropic transition. We further restrict the deformation temperature to 10 °C to separate the two shape-change mechanisms. An even lower programming temperature may require a large force that is beyond the capacity of the facility. Figure 7 shows the shape-memory cycle under an applied stress of 150 kPa. The programmed shape is fixed through cooling to low temperatures, which is named programming process for SMPs. As the temperature rises, the strain begins to decrease at around 0 °C, which is caused by the shape recovery of the programmed shape. At around 35 °C, the strain reaches the minimum value and begins to increase with temperature, which is induced by the nematic-isotropic transition. The temperature region for the nematic-isotropic transition is higher than that of the shape recovery. Thus, with increasing temperature, the strain first decreases and then increases.
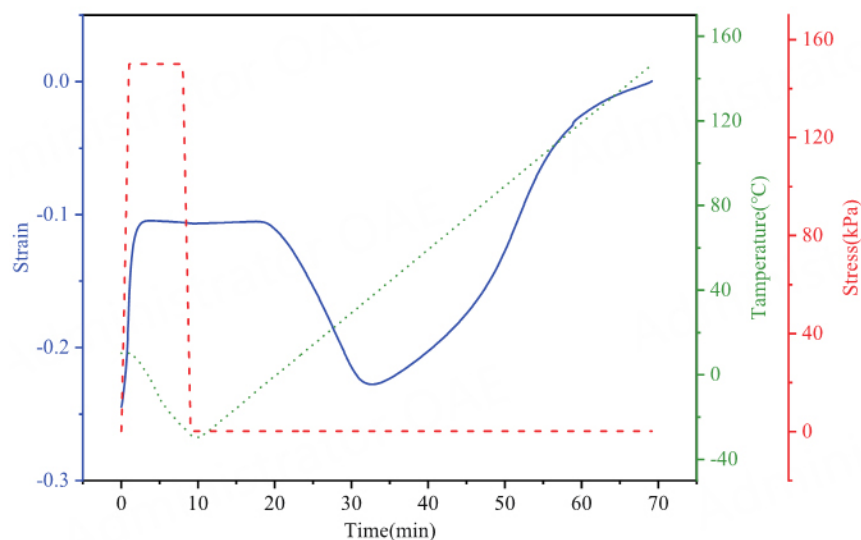
Figure 7. Shape-memory cycle for monodomain LCEs programmed at 10 °C and with an applied stress of 150 kPa. LCEs: Liquid crystal elastomers.

Figure 8 further compares the strain evolution of monodomain LCEs under different magnitudes of applied stress. It can be seen that the programmed strain also increases with the applied stress. All the curves overlap, indicating that the programmed shape has achieved a full recovery at 40 °C. The strain caused by the nematic-isotropic transition cannot be tuned. In contrast, the programmed strain increases with the applied load. Thus, when the load reaches a specific value, 200 kPa, in our tests, the magnitude of the strain decrease is the same as that of the strain increase. For a larger programmed stress, such as 250 kPa, the magnitude of the strain decrease surpasses that of the strain increase.

Since the LCEs investigated in this work have possessed a similar glass transition behavior as the traditional amorphous chemically cross-linked polymers, we demonstrate that they can exhibit an excellent one-way shape-memory effect. In addition, due to the nematic-isotropic transition, the monodomain LCEs exhibit two-way shape-memory behaviors. In the above part, we have shown that complex recovery paths can be achieved by combining the one-way and two-way shape-memory effects. The performances can be tuned by adjusting the programming temperature and stress. For our material systems, the glass transition and nematic-isotropic transition regions are not separated with a wide temperature interval. We plan to optimize the chemical structures to achieve well-separated transition regions. This can be further used to achieve the triple shape-memory effect.

A bilayer structure was also printed with a polydomain layer and a monodomain layer. Since the monodomain layer is printed with a 45° angle with respect to the length direction, the flat structure will twist with increasing temperature due to the mismatch strain between two layers, as shown in Figure 9. The twisted shape can return to the flat shape with decreasing temperature. Thus, these two shapes can transit to each other with changing temperatures, which is the same as the two-way shape-memory effect, as shown in Figure 4B. To demonstrate the one-way shape-memory effect, the bilayer was bent to an arc shape and placed in the fridge to fix this temporary shape. The structure can return to a flat shape at 35 °C due to shape recovery. A further increase in temperature can result in a twisted shape.
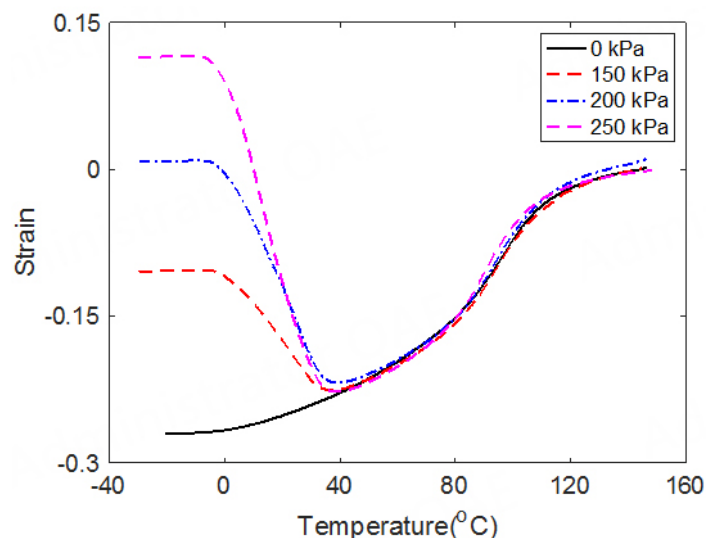
Figure 8. Shape recovery performance of monodomain LCEs with different applied stress levels. LCEs: Liquid crystal elastomers.
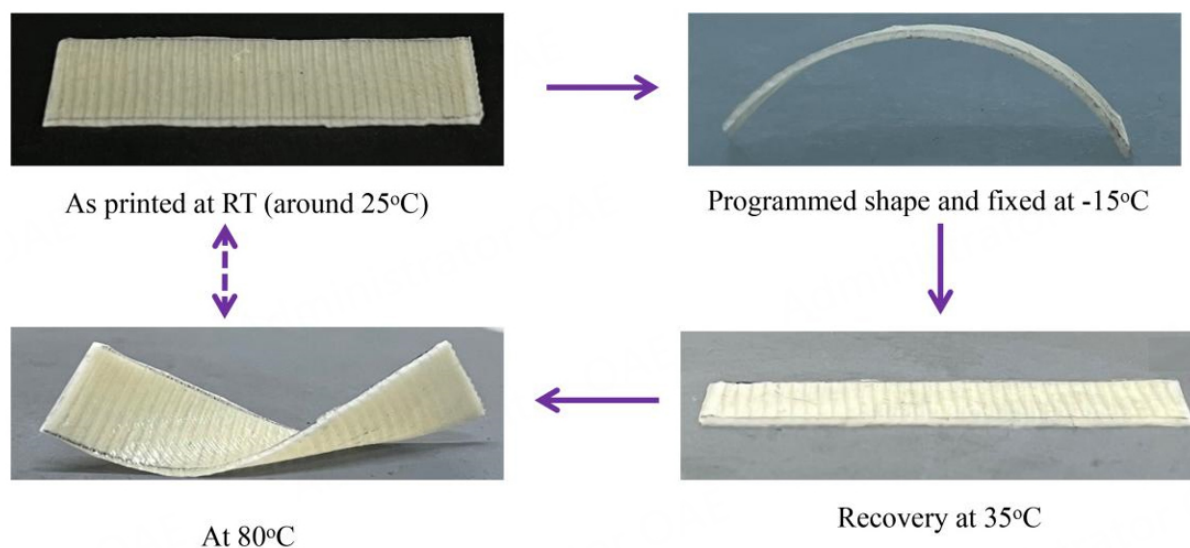
Figure 9. Demonstration of the coupling between the one-way shape-memory effect and the two-way shape-memory effect in the bilayer structure.

CONCLUSIONS

In this work, we employ the DIW 3D printing technique to fabricate LCEs. Both polydomain and monodomain LCEs can be obtained by controlling the temperature of glass substrates. The dynamic properties, such as storage modulus and loss factor tanδ, do not show much difference between the polydomain and monodomain LCEs. In contrast, the DSC tests reveal there exist both glass transition and nematic-isotropic transition in monodomain LCEs, while only the glass transition is observed in polydomain LCEs. Reversible shape change can occur for the polydomain LCEs when subject to a constant force, while the shape change for monodomain LCEs does not require any external loading. We further show that the one-way shape-memory effect can be achieved due to glass transition. For the monodomain LCEs, complex recovery behaviors, such as non-monotonic recovery paths, can be obtained by controlling the programming conditions. These findings provide more design space for employing LCEs as shape-memory materials.

DECLARATIONS

Authors' contributions
Conception and design of the study:Wang Z, Xiao R
Performed data analysis and interpretation: Dai L
Performed data acquisition: Dai L, Wang L, Chen B, Xu Z

Availability of data and materials
Not applicable.

Conflicts of interest
All authors declared that there are no conflicts of interest.

Ethical approval and consent to participate
Not applicable.

Consent for publication
Not applicable.

Copyright

REFERENCES

1.　Lendlein A, Gould OEC. Reprogrammable recovery and actuation behaviour of shape-memory polymers. *Nat Rev Mater* 2019;4:116-33. DOI

2.　Sun L, Huang W, Ding Z, et al. Stimulus-responsive shape memory materials: a review. *Mater Des* 2012;33:577-640. DOI

3.　Lei M, Chen Z, Lu H, Yu K. Recent progress in shape memory polymer composites: methods, properties, applications and prospects. *Nanotechnol Rev* 2019;8:327-51. DOI

4.　Wang YJ, Jeng US, Hsu SH. Biodegradable water-based polyurethane shape memory elastomers for bone tissue engineering. *ACS Biomater Sci Eng* 2018;4:1397-406. DOI PubMed

5.　Xue Y, Lei J, Liu Z. A thermodynamic constitutive model for shape memory polymers based on phase transition. *Polymer* 2022;243:124623. DOI

6.　Wang X, Lu H, Gorbacheva G, Hossain M, Fu YQ. Multi-modal commutative dynamics in semi-crystalline polymers undergoing multiple shape memory behavior. *Smart Mater Struct* 2021;30:045003. DOI

7.　Ramaraju H, Akman RE, Safranski DL, Hollister SJ. Designing biodegradable shape memory polymers for tissue repair. *Adv Funct Mater* 2020;30:2002014. DOI

8.　Li Z, Liu Y, Wang Y, Lu H, Lei M, Fu YQ. 3D printing of auxetic shape-memory metamaterial towards designable buckling. *Int J Appl Mech* 2021;13:2150011. DOI

9.　Liu R, Xu S, Luo X, Liu Z. Theoretical and numerical analysis of mechanical behaviors of a metamaterial-based shape memory polymer stent. *Polymers* 2020;12:1784. DOI PubMed PMC

10.　Zhang D, Liu L, Xu P, et al. World's first application of a self-deployable mechanism based on shape memory polymer composites in Mars explorations: ground-based validation and on-Mars qualification. *Smart Mater Struct* 2022;31:115008. DOI

11.　Xiao R, Huang WM. Heating/Solvent responsive shape-memory polymers for implant biomedical devices in minimally invasive surgery: current status and challenge. *Macromol Biosci* 2020;20:e2000108. DOI PubMed

12.　Delaey J, Dubruel P, Van Vlierberghe S. Shape-memory polymers for biomedical applications. *Adv Funct Mater* 2020;30:1909047.

DOI

13. Salaris V, Leonés A, Lopez D, Kenny JM, Peponi L. Shape-memory materials via electrospinning: a review. *Polymers* 2022;14:995. DOI PubMed PMC

14. Zhang B, Li H, Cheng J, et al. Mechanically robust and UV-curable shape-memory polymers for digital light processing based 4D printing. *Adv Mater* 2021;33:e2101298. DOI PubMed

15. Bastola AK, Hossain M. The shape - morphing performance of magnetoactive soft materials. *Mater Des* 2021;211:110172. DOI

16. Lin C, Lv J, Li Y, et al. 4D-Printed biodegradable and remotely controllable shape memory occlusion devices. *Adv Funct Mater* 2019;29:1906569. DOI

17. Zhao D, Han C, Peng B, et al. Corrosion fatigue behavior and anti-fatigue mechanisms of an additively manufactured biodegradable zinc-magnesium gyroid scaffold. *Acta Biomater* 2022;153:614-29. DOI PubMed

18. Sun S, Teng Q, Xie Y, et al. Two-step heat treatment for laser powder bed fusion of a nickel-based superalloy with simultaneously enhanced tensile strength and ductility. *Addit Manuf* 2021;46:102168. DOI

19. Cai C, Qiu JCD, Shian TW, et al. Laser powder bed fusion of Mo_2C/Ti-6Al-4V composites with alternately laminated α′/β phases for enhanced mechanical properties. *Addit Manuf* 2021;46:102134. DOI

20. Zhao D, Liang H, Han C, et al. 3D printing of a titanium-tantalum Gyroid scaffold with superb elastic admissible strain, bioactivity and in-situ bone regeneration capability. *Addit Manuf* 2021;47:102223. DOI

21. Wang K, Jia Y, Zhu XX. Two-way reversible shape memory polymers made of cross-linked cocrystallizable random copolymers with tunable actuation temperatures. *Macromolecules* 2017;50:8570-9. DOI

22. Zare M, Prabhakaran MP, Parvin N, Ramakrishna S. Thermally-induced two-way shape memory polymers: mechanisms, structures, and applications. *Chem Eng J* 2019;374:706-20. DOI

23. Chung T, Romo-uribe A, Mather PT. Two-way reversible shape memory in a semicrystalline network. *Macromolecules* 2008;41:184-92. DOI

24. Behl M, Kratz K, Noechel U, Sauter T, Lendlein A. Temperature-memory polymer actuators. *Proc Natl Acad Sci USA* 2013;110:12555-9. DOI

25. Song H, Fang Z, Jin B, Pan P, Zhao Q, Xie T. Synergetic chemical and physical programming for reversible shape memory effect in a dynamic covalent network with two crystalline phases. *ACS Macro Lett* 2019;8:682-6. DOI PubMed

26. Wang Z, Wang Z, Zheng Y, He Q, Wang Y, Cai S. Three-dimensional printing of functionally graded liquid crystal elastomer. *Sci Adv* 2020;6. DOI PubMed PMC

27. Herbert KM, Fowler HE, Mccracken JM, Schlafmann KR, Koch JA, White TJ. Synthesis and alignment of liquid crystalline elastomers. *Nat Rev Mater* 2022;7:23-38. DOI

28. Yakacki CM, Saed M, Nair DP, Gong T, Reed SM, Bowman CN. Tailorable and programmable liquid-crystalline elastomers using a two-stage thiol-acrylate reaction. *RSC Adv* 2015;5:18997-9001. DOI

29. Wen Z, Yang K, Raquez JM. A review on liquid crystal polymers in free-standing reversible shape memory materials. *Molecules* 2020;25:1241. DOI PubMed PMC

30. Fuchi K, Ware TH, Buskohl PR, et al. Topology optimization for the design of folding liquid crystal elastomer actuators. *Soft Matter* 2015;11:7288-95. DOI PubMed

31. Roach DJ, Yuan C, Kuang X, et al. Long liquid crystal elastomer fibers with large reversible actuation strains for smart textiles and artificial muscles. *ACS Appl Mater Interfaces* 2019;11:19514-21. DOI PubMed

32. Wang Z, Guo Y, Cai S, Yang J. Three-dimensional printing of liquid crystal elastomers and their applications. *ACS Appl Polym Mater* 2022;4:3153-68. DOI

33. Spillmann CM, Naciri J, Ratna BR, Selinger RL, Selinger JV. Electrically induced twist in smectic liquid-crystalline elastomers. *J Phys Chem B* 2016;120:6368-72. DOI PubMed

34. Wang Z, He Q, Wang Y, Cai S. Programmable actuation of liquid crystal elastomers via "living" exchange reaction. *Soft Matter* 2019;15:2811-6. DOI

35. Saed MO, Gablier A, Terentjev EM. Exchangeable liquid crystalline elastomers and their applications. *Chem Rev* 2022;122:4927-45. DOI PubMed PMC

36. Peng X, Wu S, Sun X, et al. 4D Printing of freestanding liquid crystal elastomers via hybrid additive manufacturing. *Adv Mater* 2022;34:e2204890. DOI PubMed

37. Traugutt NA, Mistry D, Luo C, Yu K, Ge Q, Yakacki CM. Liquid-crystal-elastomer-based dissipative structures by digital light processing 3D printing. *Adv Mater* 2020;32:e2000797. DOI PubMed

38. Saed MO, Torbati AH, Starr CA, Visvanathan R, Clark NA, Yakacki CM. Thiol-acrylate main-chain liquid-crystalline elastomers with tunable thermomechanical properties and actuation strain. *J Polym Sci Part B Polym Phys* 2017;55:157-68. DOI

39. Chen G, Jin B, Shi Y, Zhao Q, Shen Y, Xie T. Rapidly and repeatedly reprogrammable liquid crystalline elastomer via a shape memory mechanism. *Adv Mater* 2022;34:e2201679. DOI PubMed

40. Javed M, Corazao T, Saed MO, et al. Programmable shape change in semicrystalline liquid crystal elastomers. *ACS Appl Mater Interfaces* 2022;14:35087-96. DOI PubMed

41. Kotikian A, Truby RL, Boley JW, White TJ, Lewis JA. 3D printing of liquid crystal elastomeric actuators with spatially programed nematic order. *Adv Mater* 2018;30:1706164. DOI PubMed

42. Huang WM, Zhao Y, Wang CC, et al. Thermo/chemo-responsive shape memory effect in polymers: a sketch of working mechanisms,

fundamentals and optimization. *J Polym Res* 2012:19. DOI

43.   Linares CP, Traugutt NA, Saed MO, Martin Linares A, Yakacki CM, Nguyen TD. The effect of alignment on the rate-dependent behavior of a main-chain liquid crystal elastomer. *Soft Matter* 2020;16:8782-98. DOI PubMed

44.   Chen SJ, Hu JL, Chen SG, Zhang CL. Study on the structure and morphology of supramolecular shape memory polyurethane containing pyridine moieties. *Smart Mater Struct* 2011;20:065003. DOI

45.   Yu K, Qi HJ. Temperature memory effect in amorphous shape memory polymers. *Soft Matter* 2014;10:9423-32. DOI PubMed